

Alma Mater Studiorum Università di Bologna  
Archivio istituzionale della ricerca

Electrical and Mechanical Properties of Electrospun PVDF-HFP with ZrO<sub>2</sub> Nanoparticles Used as Separator in Electrochemical Systems

This is the final peer-reviewed author's accepted manuscript (postprint) of the following publication:

*Published Version:*

L. Gasperini, S. Gandolfi, S.V. Suraci, D. Fabiani (2023). Electrical and Mechanical Properties of Electrospun PVDF-HFP with ZrO<sub>2</sub> Nanoparticles Used as Separator in Electrochemical Systems. Piscataway, NJ : IEEE [10.1109/CEIDP51414.2023.10410461].

*Availability:*

This version is available at: <https://hdl.handle.net/11585/955578> since: 2024-02-05

*Published:*

DOI: <http://doi.org/10.1109/CEIDP51414.2023.10410461>

*Terms of use:*

Some rights reserved. The terms and conditions for the reuse of this version of the manuscript are specified in the publishing policy. For all terms of use and more information see the publisher's website.

This item was downloaded from IRIS Università di Bologna (<https://cris.unibo.it/>).  
When citing, please refer to the published version.

(Article begins on next page)

# Electrical and mechanical properties of electrospun PVDF-HFP with ZrO<sub>2</sub> nanoparticles for energy storage systems

L. Gasperini, S. Gandolfi, S.V. Suraci, D. Fabiani

LIMES - Department of Electrical, Electronic and Information Engineering (DEI)  
University of Bologna, Bologna Italy

**Abstract-** This study focuses on the preparation of nanocomposite polymer membranes by the electrospinning technique. PVDF-HFP polymer was combined with different concentrations of ZrO<sub>2</sub> (0, 5, 7, and 10 wt%). The fabricated nanofibrous membranes were analyzed to evaluate their electrochemical and mechanical properties. The incorporation of the ceramic filler was investigated to determine its influence on the separator performance, aiming to develop high-performance separators for future Energy Storage Systems (ESSs).

## I. INTRODUCTION

Energy storage systems (ESSs) have gained significant importance in modern energy infrastructure due to their ability to store and release energy as needed. Among the various components that comprise an ESS, separators play a crucial role in ensuring efficient and safe operation. These separators are thin, porous membranes that physically separate the positive and negative electrodes of the energy storage system, preventing direct contact and electrical short circuits and minimizing the risk of thermal runaway. The importance of separators lies in their ability to enhance the overall performance, reliability, and safety of the system. In particular, separators offer a degree of thermal and chemical stability, helping to maintain the structural integrity of the system under various operating conditions.

The main categories of battery separators include single polymer separators, composite separators, and polymer blends. In the area of separator membranes, significant research has been devoted to poly(vinylidene fluoride) (PVDF) and its copolymers due to their processability with various techniques (e.g. solvent casting and electrospinning), chemical inertness, and high-stress stability [1], [2]. Moreover, these materials exhibit strong polarity (high dipolar moment), controllable crystallinity, and high dielectric properties, which contribute to enhance ionization of lithium salts.

Currently, polymer membrane produced via electrospinning have garnered significant attention due to their three-dimensional interconnected porous structure. This unique structure enables several advantageous characteristics, including high electrolyte uptake, enhanced ionic mobility, excellent dimensional stability, and prevention of electrolyte leakage. However, the mechanical properties of such materials are quite poor to withstand the stresses occurring during battery fabrication. Therefore, recent research has been directed

towards enhancing the mechanical performance by incorporating nanoscale filler particles. These additives can be dispersed within the polymer matrix or deposited on the surface of the nanofibers themselves using suitable techniques, such as electrostatic spray deposition [3]. Commonly employed additives in energy storage separators include ferroelectric materials, such as barium titanate (BaTiO<sub>3</sub>), carbon fillers and inert ceramic oxides. Ceramic additives generally strengthen the mechanical properties of the separator due to their ability to withstand high temperatures and provide improved thermal stability. Among those ones, the most widely used are aluminum oxide (Al<sub>2</sub>O<sub>3</sub>), silicon dioxide (SiO<sub>2</sub>) and zirconium dioxide (ZrO<sub>2</sub>). Numerous studies have demonstrated the improvements achieved by incorporating silica in different compositions in lithium/lithium iron phosphate batteries (Li/LiFePO<sub>4</sub>) [4], [5]. Zirconium oxide is another significant additive that, even in small quantities, significantly enhances the thermal and mechanical properties of a polymeric separator due to its ceramic filler nature [6].

Nonetheless, despite some notable improvements, comprehensive analyses on the use of ZrO<sub>2</sub> as a ceramic filler are lacking in literature, particularly on the mechanical and electrical performance of the nanoadditive separator. Thus, this study aims at investigating the electrical and mechanical properties of a poly(vinylidene fluoride-co-hexafluoropropylene) (PVDF-HFP) nanofibrous membrane for ESSs while varying the concentration of zirconia as a nanofiller to enhance the separator performance.

## II. MATERIALS AND METHODS

### A. Specimen Manufacturing Process

The nanofibrous membranes were fabricated using the electrospinning technique, starting with the preparation of a polymeric solution. Initially, zirconium oxide nanopowders (ZrO<sub>2</sub> average diameter: 30 nm, Nanografi Nano Technology) were dissolved in N, N'-dimethyl acetamide (DMAc). To achieve a homogeneous suspension, a sonicator (Hielscher UP200St) operating at 50 W for 30 minutes was employed. To minimize solvent evaporation, the sonication process was conducted in an ice bath. Three distinct solutions were prepared by combining PVDF-HFP (Kynar flex 2801, Arkema, Mw = 4.77×10<sup>5</sup>) at a concentration of 16 wt% with ZrO<sub>2</sub> at 5, 7, and 10 wt%. Acetone (AC) and DMAc were used as solvents in a

weight ratio of 70:30. To ensure complete mixing, the solutions were stirred for 5 hours.

The electrospinning apparatus (Spinbow Lab Unit, Spinbow S.r.l., Italy) consists of four high voltage needles and a low-speed rotating drum collector connected to the ground. The polymeric solution was pumped at a flow rate of 1.3 ml/h and high voltage (20kV) was applied to the needles. Distance between the tip of the needle and the drum collector was set to 15 cm. In Table I are reported the four different samples manufactured via electrospinning.

TABLE I  
MANUFACTURED SAMPLES

	PVDF-HFP	PVDF-HFP + 5 wt% ZrO <sub>2</sub>	PVDF-HFP + 7 wt% ZrO <sub>2</sub>	PVDF-HFP + 10 wt% ZrO <sub>2</sub>
Sample	1	2	3	4

#### B. Electronic Conductivity Measurements

To perform the electrical conductivity tests, four films were fabricated using the non-solvent induced phase separation (NIPS) technique. The films included pure PVDF-HFP as well as PVDF-HFP with the addition of 5, 7, and 10 wt% zirconium oxide. The casting solution was stirred continuously at room temperature for 12 hours. The solution was initially cast onto a dry and clean glass substrate using a casting blade, ensuring a controlled polymer film thickness of about 200  $\mu\text{m}$ . Subsequently, the glass substrate with the wet-cast polymer film was immersed for 15 minutes in a coagulation bath consisting of a mixture of isopropyl alcohol (IPA) and DMAc in a weight ratio of 70:30. Then, the polymer film was transferred to a IPA bath and soaked for 20 min and then in a deionized water bath for other 5 minutes. Finally, the separator was dried at 80  $^{\circ}\text{C}$  for 12 hours to remove residual water and solvents.

According to the guidelines reported in ASTM D257-14 (2021), accurate electronic conductivity measurements require the use of a specific electrode system to effectively measure the current flowing through the sample under test. This electrode system includes a grounded protective ring, which is designed to prevent any potential leakage current from the surface being measured. To obtain the desired electrode system, a thin layer of gold is deposited on the sample surface by a cold sputtering metallization process in accordance with the required geometry (HV electrode diameter of 25 mm, low voltage electrode diameter of 20 mm and grounded guard ring of 25 mm). After electrode deposition, the metallized samples are grounded for at least 24 hours in air to remove any residual charge. The electronic conductivity tests were performed using a Keithly 2290E-5 5kV DC generator to apply the required voltage and a Keysight B2981A picoamperemeter to registers the current passing through the sample under test [7]. Following the averaging of the current measured at steady state conditions ( $i_{\text{cond}}$ ), conductivity was obtained:

$$\sigma_e = J/E \quad [\text{S/m}] \quad (1)$$

where  $J$  is the conduction current density (given by the ratio between  $i_{\text{cond}}$  and the electrode surface  $S$ ) and  $E$  is the electric field, set equal to 1 kV/mm.

#### C. Ionic Conductivity Measurements

The resistivity of the electrolyte-saturated membranes was determined by means of electrochemical impedance spectroscopy (EIS). For this purpose, a Solartron SI 1255 frequency response analyzer coupled with an EG&G Model 273A PAR potentiostat/galvanostat and Biologic VSP was used. In the EIS analysis, the separator, previously soaked in the electrolyte, was placed inside a T-shaped Teflon cell (BOLA by Bohlender GmbH) sandwiched between two stainless steel (SS) blocking electrodes with an area of 0.785  $\text{cm}^2$ , arranged in a symmetrical configuration. EIS measurements involved applying an AC perturbation of 5 mV, with a frequency between 100 kHz and 100 mHz. The MacMullin number is a parameter which considers separator contribution to the internal resistance and was calculated as follows:

$$N_M = \rho_{s+e}/\rho_e \quad (2)$$

where  $\rho_{s+e}$  represents the resistivity of the electrolyte/separator assembly under consideration and  $\rho_e$  the resistivity of the electrolyte solutions (LP30 with a resistivity of 82.5  $\Omega\cdot\text{cm}$  [8]). A low MacMullin number indicates low internal resistance, resulting in improved battery efficiency. Ideally, this number should approach one. However, commercial membrane separators typically have MacMullin numbers between 15 and 17, mainly due to the porosity of the film, which is about 40 percent.

#### D. Mechanical Characterization

Two types of mechanical test, tensile tests and thermal shrinkage, were performed on the nanofibrous membrane of Table I to evaluate the effect of ceramic nanoadditives. Tensile tests were conducted using a Remet TC10 universal testing machine, which was equipped with a 10 N load cell. The tests were performed at a crosshead separation speed of 10 mm/min. To ensure better handling and prevent slippage of nanofibers in the machine fixtures, the tensile specimens were prepared by anchoring the membrane to a paper frame (47×67 and 25×45 mm outer and inner dimensions, respectively). The frame was then cut before the start of the test, as previously described in [9]. After tensile test, the sample was retrieved and weighted to calculate the stress ( $\sigma_m$ ) as:

$$\sigma_m = \rho_m \cdot F \cdot L_0 / m \quad [\text{MPa}] \quad (3)$$

where  $\rho_m$  is the material density ( $\text{mg}/\text{mm}^3$ ),  $m$  is the tested sample mass (mg),  $L_0$  is the specimen initial length (mm) and  $F$  is the applied force (N). Stress-strain graphs were obtained from a minimum of five samples for each type of nanofibrous mat. The strain ( $\epsilon$ ) was determined as follows:.

$$\varepsilon = L - L_0/L_0 \quad (4)$$

where  $L - L_0$  is the change in length observed during the test. The elastic modulus ( $E$ ) is determined by calculating the slope of the tangent to the initial linear region of the stress-strain curve.

The thermal stability of the nanofibrous separator of Table I was evaluated by measuring the shrinkage,  $A$ , of a 20-mm diameter round sample by using the following equation:

$$A = (D_0 - D)/D_0 \cdot 100 \quad (5)$$

where  $D_0$  and  $D$  are the diameter of the sample before and after the thermal test, respectively. The experiments were conducted within a temperature range from 50 to 150 °C in 20 °C intervals, each test lasting 30 minutes.

### III. RESULTS AND DISCUSSION

#### A. Micrograph Analyses

The nanofibrous layers produced through the electrospinning process were examined using Scanning Electron Microscopy (SEM), as reported in Fig. 1. The micrograph analyses reveal that an increase in  $ZrO_2$  concentration leads to a corresponding increase in the average diameter of the nanofibers. Furthermore, the zirconia particles are initially observed to be deposited on the surface of the polymer fibers, gradually forming a distinct layer that completely covers the PVDF-HFP nanofibers. This behavior is particularly evident in the case of the separator with a 10 wt% concentration of zirconia (Fig. 1 c))

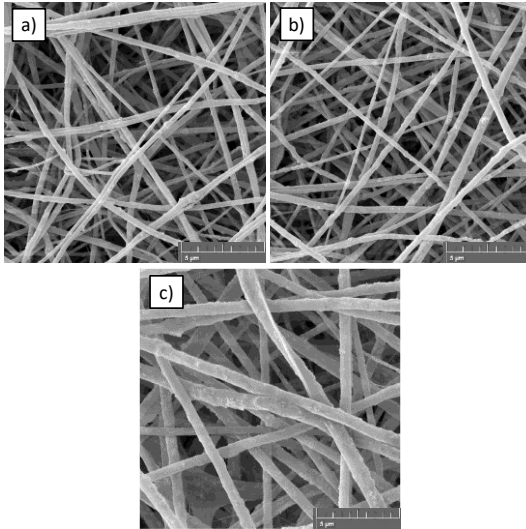


Fig. 1. SEM micrograph analyses of PVDF-HFP nanofibers with different amount of  $ZrO_2$ : a) 5 wt%, b) 7 wt%, c) 10 wt%

#### B. Electronic and Ionic Conductivity

Fig. 2 reports the values of calculated conductivity obtained through the current measurements, for neat PVDF-HFP and PVDF-HFP with different amount of  $ZrO_2$ , respectively.

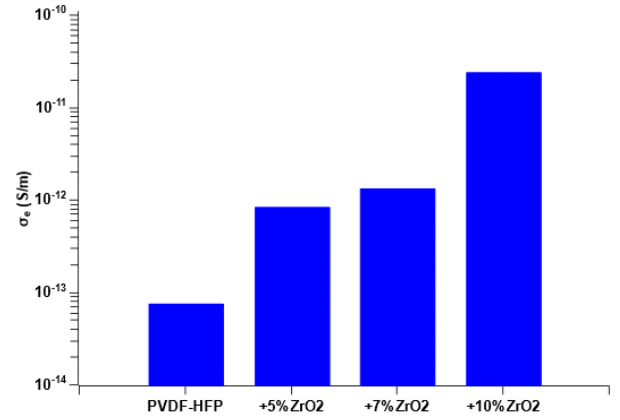


Fig. 2. Electronic conductivity at different amount of  $ZrO_2$

The results demonstrate that the electronic conductivity increases with an increasing percentage of zirconia. However, for concentrations below 7%, the conductivity remains relatively low. Interestingly, in the case of the 10 percent sample, a significant increase of more than one order of magnitude in conductivity is observed. This suggests that the separator may exhibit non-ideal behavior for ESS applications, permitting the conduction of a significantly higher number of electrons.

Resistivities of the electrolyte-separator system were determined through EIS measurements, and the corresponding MacMullin numbers were calculated. The results, shown in Table II, indicate that there is minimal variation in the  $N_M$  among different types of separators. In particular, the nanofibrous separators exhibit significantly lower MacMullin numbers compared to traditional membranes such as Celgard 2400 (16).

TABLE II  
MACMULLIN NUMBER

	PVDF-HFP	PVDF-HFP + 5 wt% $ZrO_2$	PVDF-HFP + 7 wt% $ZrO_2$	PVDF-HFP + 10 wt% $ZrO_2$
$N_M$	3.2	4.4	4.8	3.5

#### C. Mechanical Performances

Table III presents the maximum stress ( $\sigma_{MAX}$ ), the maximum elongation to failure ( $\varepsilon_{MAX}$ ) and the elastic modulus ( $E$ ) values of the four nanofibrous membranes. These values were derived from the stress-strain curves obtained during the tensile tests performed on the samples.

TABLE III  
TENSILE TEST RESULTS

	PVDF-HFP	PVDF-HFP + 5 wt% $ZrO_2$	PVDF-HFP + 7 wt% $ZrO_2$	PVDF-HFP + 10 wt% $ZrO_2$
$\sigma_{MAX}$ (MPa)	26.3 ± 1.2	31.2 ± 1.4	29.1 ± 0.8	27.7 ± 1.2
$\varepsilon_{MAX}$ (%)	157 ± 7	134 ± 2	137 ± 6	133 ± 6
$E$ (MPa)	141.6 ± 5.3	152.3 ± 18	237.4 ± 8.2	223.5 ± 11.4

The incorporation of the ceramic nanoadditives leads to an increase in maximum bearable stress, reaching a peak in the

case of the 5 wt% ZrO<sub>2</sub> specimens. However, the maximum elongation decreases compared to the pure PVDF-HFP specimen. Additionally, the Young modulus shows an increase compared to neat PVDF, indicating an improvement in stiffness attributed to the presence of the ceramic additive. Focusing on the application as a separator, the property to take into account is the maximum strength, since it would ensure a better mechanical resistance, allowing the separator to withstand the high stresses involved in battery assembly.

The thermal stability of nanofibrous membranes was assessed by evaluating their thermal shrinkage. In the temperature range of 50 to 110 °C, no remarkable changes in the samples were noted. However, at temperatures of 130 °C and especially at 150 °C, significant shrinkage was observed in the case of pure PVDF-HFP. This would be a problem since in case of thermal runaway due to high currents, the storage system could easily short-circuit. Table IV presents the percent shrinkage values of the samples at 150 °C. It is worth noting that the samples with added nanoparticles exhibited lower thermal shrinkage, with a significant difference of up to 40 percent compared to pure PVDF-HFP in the case of the 7 wt% zirconium oxide specimen (Fig. 3).

TABLE IV  
THERMAL SHRINKAGE

	PVDF-HFP	PVDF-HFP + 5 wt% ZrO <sub>2</sub>	PVDF-HFP + 7 wt% ZrO <sub>2</sub>	PVDF-HFP + 10 wt% ZrO <sub>2</sub>
A (%)	65.9	34.7	25.4	35.7

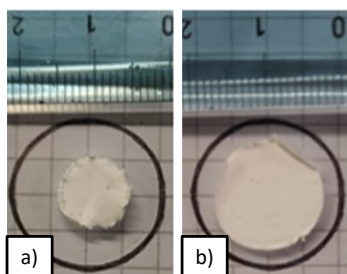


Fig. 3. Pure PVDF-HFP a) and PVDF-HFP + 7% of ZrO<sub>2</sub> b) after 30 minutes of thermal treatment at 150 °C

#### IV. CONCLUSIONS

PVDF-HFP nanofibrous separators with different percentages of ZrO<sub>2</sub> were fabricated using the electrospinning technique. SEM analysis revealed that the integration of zirconium oxide with the nanofibers generating a coating, thus results in an increased average diameter of the PVDF-HFP fibers. In terms of electrical conductivity, a significant increase was observed, particularly for the sample containing 10 wt% of ZrO<sub>2</sub>, exhibiting a conductivity two orders of magnitude higher than the non-additive specimen.

Interestingly, the MacMullin number exhibited minimal variation with changing zirconia percentages and remained considerably low compared to conventional polymer membranes used in energy storage systems. The incorporation of nanoadditives also influenced the mechanical properties of the separator. While the maximum elongation at break

decreased, the maximum stress and elastic modulus increased with the addition of the ceramic additive. This indicates a stiffer material capable of withstanding higher stresses.

Furthermore, the addition of ceramic materials improved the thermal stability of the separator, resulting in reduced shrinkage. This advantage mitigates the risk of potential short circuits that may occur during thermal runaway. Overall, these results demonstrate that the incorporation of ceramic nanofillers enhances the performance of the separator, thereby paving the way to the development of high-performance separators for future energy storage systems. In particular, the concentration of ~5%wt of ZrO<sub>2</sub> is found to optimize all the material properties under consideration i.e., electrical, and mechanical ones.

Future research in this field will include further investigation of the electrical and mechanical characteristics of the material. This investigation will involve examining changes in conductivity with temperature and performing puncture tests on the nanofibrous membrane.

#### ACKNOWLEDGMENT

The authors are grateful to Dr. Maccaferri and Prof. Arbizzani for helping performing the tensile and ionic conductivity tests.

#### REFERENCES

- [1] C. M. Costa and S. Lanceros-Mendez, "Recent advances on battery separators based on poly(vinylidene fluoride) and its copolymers for lithium-ion battery applications," *Curr. Opin. Electrochem.*, vol. 29, p. 100752, 2021, doi: 10.1016/j.coelec.2021.100752.
- [2] C. M. Costa, M. M. Silva, and S. Lanceros-Méndez, "Battery separators based on vinylidene fluoride (VDF) polymers and copolymers for lithium ion battery applications," *RSC Adv.*, vol. 3, no. 29, pp. 11404–11417, 2013, doi: 10.1039/c3ra40732b.
- [3] B. Yu, X. M. Zhao, X. N. Jiao, and D. Y. Qi, "Composite nanofiber membrane for lithium-ion batteries prepared by electrostatic spun/spray deposition," *J. Electrochem. Energy Convers. Storage*, vol. 13, no. 1, pp. 1–6, 2016, doi: 10.1115/1.4034030.
- [4] J. K. Kim, G. Cheruvally, X. Li, J. H. Ahn, K. W. Kim, and H. J. Ahn, "Preparation and electrochemical characterization of electrospun, microporous membrane-based composite polymer electrolytes for lithium batteries," *J. Power Sources*, vol. 178, no. 2, pp. 815–820, 2008, doi: 10.1016/j.jpowsour.2007.08.063.
- [5] P. Raghavan *et al.*, "Novel electrospun poly(vinylidene fluoride-co-hexafluoropropylene)-in situ SiO<sub>2</sub> composite membrane-based polymer electrolyte for lithium batteries," *J. Power Sources*, vol. 184, no. 2, pp. 437–443, 2008, doi: 10.1016/j.jpowsour.2008.03.027.
- [6] A. K. Solarajan, V. Murugadoss, and S. Angaiah, "Dimensional stability and electrochemical behaviour of ZrO<sub>2</sub> incorporated electrospun PVdF-HFP based nanocomposite polymer membrane electrolyte for Li-ion capacitors," *Sci. Rep.*, vol. 7, no. February, pp. 1–10, 2017, doi: 10.1038/srep45390.
- [7] S. Hettal, S. V. Suraci, S. Roland, D. Fabiani, and X. Colin, "Towards a Kinetic Modeling of the Changes in the Electrical Properties of Cable Insulation During Radio-Thermal Ageing in Nuclear Power Plants. Application to Silane-Crosslinked Polyethylene," *Polymers (Basel)*, vol. 13, no. 24, 2021, doi: 10.3390/polym13244427.
- [8] A. Terella *et al.*, "Functional separators for the batteries of the future," *J. Power Sources*, vol. 449, no. November 2019, p. 227556, 2020, doi: 10.1016/j.jpowsour.2019.227556.
- [9] E. Maccaferri, L. Mazzocchetti, T. Benelli, T. M. Brugo, A. Zucchelli, and L. Giorgini, "Rubbery nanofibers by co-electrospinning of almost immiscible NBR and PCL blends," *Mater. Des.*, vol. 186, p. 108210, 2020, doi: 10.1016/j.matdes.2019.108210.